

SUPPORTING INFORMATION FOR

Locking water molecules via ternary O-H···O intramolecular hydrogen bonds in perhydroxylated *closo*-dodecaborate

Yanrong Jiang,^{a, b} Zhubin Hu,^b Cheng Zhong,^d Yan Yang,^b Xue-Bin Wang,^c Zhenrong
Sun,^b Haitao Sun,^{*b} Zhi Liu^{*a} and Peng Peng^{*a}

^a *Center for Transformative Science, ShanghaiTech University,
Shanghai 201210, China*

^b *State Key Laboratory of Precision Spectroscopy,
East China Normal University, Shanghai 200241, China*

^c *Physical Sciences Division, Pacific Northwest National Laboratory,
902 Battelle Boulevard, P.O. Box 999, Richland, Washington 99352, USA*

^d *College of Chemistry & Molecular Sciences,*

Wuhan University, Wuhan Hubei 430072, China

Author to whom correspondence should be addressed:

pengpeng@shanghaitech.edu.cn (P. P.); liuzhi@shanghaitech.edu.cn (Z. L.);

htsun@phy.ecnu.edu.cn (H. S.)

Computational Details

Force-field molecular dynamics simulations. All parameters for the bonded interactions were obtained from density function theory. The bond distance and angles were obtained with PBE0 using aug-cc-pVTZ basis set. The fitting electrostatic potential charges were obtained by Multiwfn²⁴. The parameters for the stretching and bending modes and the optimized Lennard-Jones (LJ) parameters were also obtained by Sobtop tool.¹ All simulations and analyses of trajectories were conducted using the GROMACS code.² The SPC/E³ water molecules were adopted in the initial configuration of the water-caged borane system, then two Na⁺ cations were added to neutralize the overall charge. The square simulation box was $5.0 \times 5.0 \times 5.0 \text{ \AA}^3$ filled up with more than 4000 water molecules. 3-dimensional periodic boundary conditions were employed. After the whole system energy minimization with a conjugate gradient algorithm, the system was then gently heated from 0 to 298.15 K in 100 ps in the NVT ensemble and then equilibrated for another 2 ns. The production run of trajectories lasted 10 ns for analyzing the configurational structure properties. A constant temperature and pressure setting with the temperature coupled to the V-rescale⁴ thermostat at 298.15 K and the pressure referenced to 1 bar using Berendsen⁵ pressure coupling was employed. The coupling constants for temperature and pressure were 0.2 and 2.5 ps, respectively, and the compressibility was fixed to $4.5 \times 10^{-5} \text{ bar}^{-1}$. For hydrogen bonded systems, the bonds with H-atoms were constrained with the LINCS⁶ constraints algorithm applied. The cut-off radius for Coulomb and Van der Waals interactions were both 1.0 nm. The long-range corrections of electrostatics was conducted by the PME⁷ method. A Maxwell distribution at 298.15 K of the studied system was initialized. A time step of 1 fs was used in the simulations.

Ab initio molecular dynamics simulations. Ab initio molecular dynamics (AIMD) simulations were performed using the ORCA 5.0.3 code.⁸ The B97-3C method was employed during the AIMD process, which show good balance between the computational cost and accuracy in describing the noncovalent interactions.⁹ The most stable configuration of each cluster was employed as the initial position and the atom velocities were initialized by the Maxwell-Boltzmann distribution at the corresponding

temperatures. A time step of 0.5 fs was set and a time constant of 30 fs was employed for canonical sampling through velocity rescaling (CSVR)⁴ to maintain the system temperature. A simulation of 30ps for each monohydrated cluster was performed and configurations were sampled every 0.5fs. Finally, the trajectory of the last 20ns of each simulation was used for analysis. The representative 2000 fs trajectories taken out from a total of 30 ps dynamic trajectories were calculated under a range of temperatures.

Table S1. Calculated vertical detachment energies (VDEs) using PBE0 and IP-EOM-DLPNO-CCSD methods with the aug-cc-pVTZ basis set for the three lowest-lying structures of $B_{12}H_{12-m}(OH)_m^{2-} \cdot nH_2O$ ($m = 0, 1, 12$; $n = 1-6$) (in eV).

			1H ₂ O	2H ₂ O	3H ₂ O	4H ₂ O	5H ₂ O	6H ₂ O
B ₁₂ H ₁₂ ²⁻	isomer 1	IP	1.63	1.90	2.13	2.36	2.49	2.77
		PBE0	1.61	1.88	2.11	2.34	2.46	2.75
	isomer 2	IP	/	1.95	2.16	2.19	2.47	2.66
		PBE0	/	1.93	2.17	2.16	2.44	2.63
	isomer 3	IP	/	1.94	2.05	2.27	2.38	2.69
		PBE0	/	1.92	2.02	2.24	2.35	2.66
B ₁₂ H ₁₁ OH ²⁻	isomer 1	IP	1.27	1.65	1.92	2.19	2.19	2.39
		PBE0	1.19	1.59	1.87	2.14	2.13	2.33
	isomer 2	IP	1.11	1.57	1.94	2.12	2.35	2.34
		PBE0	1.00	1.49	1.88	2.07	2.30	2.27
	isomer 3	IP	1.11	1.56	1.85	2.08	2.05	2.27
		PBE0	1.00	1.49	1.79	2.02	1.96	2.30
B ₁₂ (OH) ₁₂ ²⁻	isomer 1	IP	0.73	0.87	1.04	1.25	1.29	1.53
		PBE0	0.60	0.74	0.91	1.13	1.16	1.40
	isomer 2	IP	0.75	0.97	1.06	1.23	1.45	1.38
		PBE0	0.63	0.84	0.93	1.11	1.32	1.25
	isomer 3	IP	0.74	0.97	1.02	1.17	1.35	1.61
		PBE0	0.61	0.82	0.90	1.04	1.22	1.49

Table S2. Electrostatic (Elst.), exchange (Exch.), induction (Ind.), and dispersion (Disp.) terms (kcal/mol) derived from energy decomposition analysis for $B_{12}H_{12-m}(OH)_m^{2-} \cdot nH_2O$ ($m = 0, 1, 12; n = 1-6$) at SAPT2+/aug-cc-pVDZ level.

$B_{12}H_{12}^{2-}$	$1H_2O$	$2H_2O$	$3H_2O$	$4H_2O$	$5H_2O$	$6H_2O$
Elst	-16.58	-29.77	-40.68	-51.27	-56.93	-71.77
Exchange	12.14	20.93	27.96	35.54	40.52	50.12
Ind.	-4.74	-8.98	-12.27	-15.16	-16.23	-19.03
Disp.	-5.14	-8.82	-12.84	-16.98	-20.52	-25.05
Total	-14.31	-26.64	-37.83	-47.88	-53.16	-65.73
$B_{12}H_{11}OH^{2-}$	$1H_2O$	$2H_2O$	$3H_2O$	$4H_2O$	$5H_2O$	$6H_2O$
Elst	-25.08	-45.22	-58.36	-70.79	-69.48	-80.75
Exchange	21.89	36.16	43.11	51.21	50.46	57.99
Ind.	-8.84	-14.27	-18.58	-22.02	-23.05	-24.08
Disp.	-6.36	-12.19	-13.68	-16.68	-17.83	-23.54
Total	-18.38	-35.52	-47.50	-58.28	-59.89	-70.38
$B_{12}(OH)_{12}^{2-}$	$1H_2O$	$2H_2O$	$3H_2O$	$4H_2O$	$5H_2O$	$6H_2O$
Elst	-35.73	-77.71	-115.67	-153.86	-194.89	-233.45
Exchange	36.53	83.56	124.96	165.35	213.75	256.64
Ind.	-11.60	-25.83	-38.55	-50.59	-64.66	-77.33
Disp.	-10.64	-22.89	-34.52	-46.06	-58.50	-70.20
Total	-21.45	-42.88	-63.78	-85.16	-104.30	-124.34

Table S3. Calculated binding energy for single-charged and double charged hydrated borane clusters $B_{12}H_{12-m}(OH)_m^{2-/ -} \cdot H_2O$ ($m = 0, 1, 12$) at the SAPT0/jun-cc-pVDZ level (in kcal/mol). The calculated ΔVDE and binding energies separately calculated at the IP-EOM-DLPNO-CCSD/aug-cc-pVTZ and SAPT2+/aug-cc-pVDZ level were also listed.

	$B_{12}H_{12} \cdot H_2O$	$B_{12}H_{11}OH \cdot H_2O$	$B_{12}(OH)_{12} \cdot H_2O$
SAPT0 / $^{2-}$	-6.23	-9.48	-16.07
SAPT0 / $^{-}$	-14.76	-19.43	-22.40
Δ SAPT0	-8.53	-9.94	-6.33
SAPT2+ / $^{2-}$	-14.31	-18.38	-21.45
Δ VDE	-7.44	-10.70	-3.49

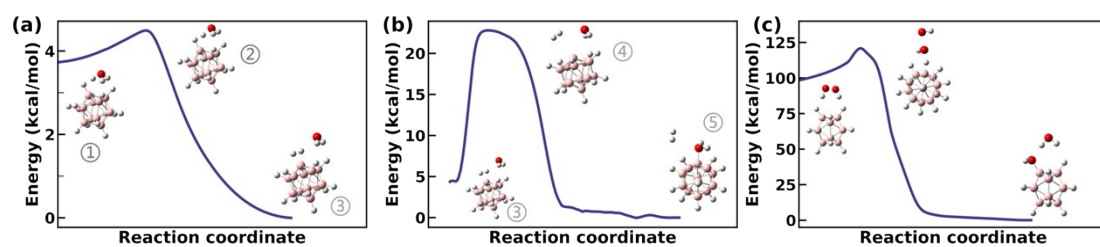


Fig. S1. Intrinsic reaction paths and energy profiles of the steps for (a) TS 1 and (b) TS 2 catalyzed by H_3O^+ under aqueous sulfuric acid and (c) TS oxidated by hydrogen peroxide during the $\text{B}_{12}\text{H}_{12}^{2-}$ mono-hydroxyl reaction calculated at PBE0/aug-cc-pVTZ level.

	H_2O	$2\text{H}_2\text{O}$	$3\text{H}_2\text{O}$	$4\text{H}_2\text{O}$	$5\text{H}_2\text{O}$	$6\text{H}_2\text{O}$		
$\text{B}_{12}\text{H}_{12}^{2-}$							isomer 1	
		0.69	0.14	0.31	0.86	0.04	isomer 2	
		0.72	0.61	0.74	3.16	0.21	isomer 3	
$\text{B}_{12}\text{H}_{11}\text{OH}^{2-}$							isomer 1	
	3.54	0.55	1.33	0.51	0.09	0.10	isomer 2	
		3.57	0.79	1.63	0.59	1.14	0.43	isomer 3
$\text{B}_{12}(\text{OH})_{12}^{2-}$							isomer 1	
	0.26	0.02	0.06	0.18	0.18	0.25	isomer 2	
		0.36	0.13	0.14	0.28	0.34	0.60	isomer 3

Fig. S2. Optimized structures of the top three lowest isomers of $\text{B}_{12}\text{H}_{12-m}(\text{OH})_m^{2-} \cdot n\text{H}_2\text{O}$ ($m = 0, 1, 12$; $n = 1-6$). Relative energies of isomers 2 and 3 (with respect to the most

stable isomer 1 in kcal/mol) calculated by DLPNO-CCSD(T)/aug-cc-pVTZ method is listed for each isomer. The water molecules are in light blue.

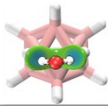

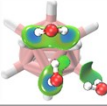
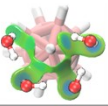
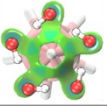
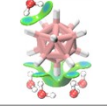

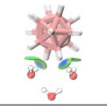

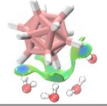
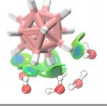

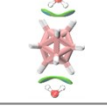
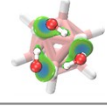
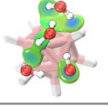
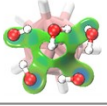
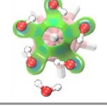

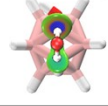
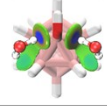

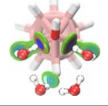
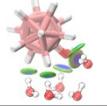
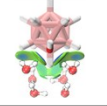
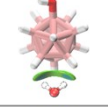
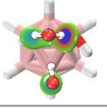

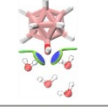
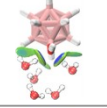
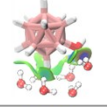
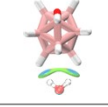
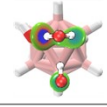
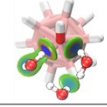
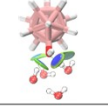
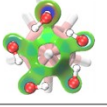
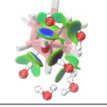
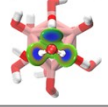
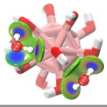
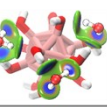
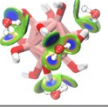
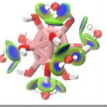
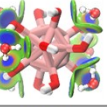
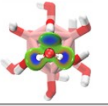
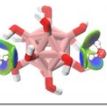
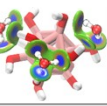
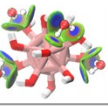
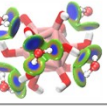
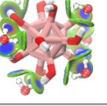
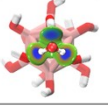
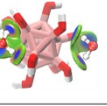
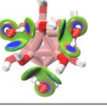
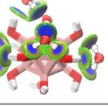
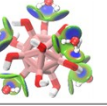
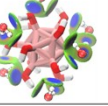
	H ₂ O	2H ₂ O	3H ₂ O	4H ₂ O	5H ₂ O	6H ₂ O	
B ₁₂ H ₁₂ ²⁻							isomer 1
		0.69	0.14	0.31	0.86	0.04	isomer 2
							
		0.72	0.61	0.74	3.16	0.21	isomer 3
							
	B ₁₂ H ₁₁ OH ²⁻						
3.54		0.55	1.33	0.51	0.09	0.10	isomer 2
							
3.57		0.79	1.63	0.59	1.14	0.43	isomer 3
							
B ₁₂ (OH) ₁₂ ²⁻							
	0.26	0.02	0.06	0.18	0.18	0.25	isomer 2
							
	0.36	0.13	0.14	0.28	0.34	0.60	isomer 3
							

Fig. S3. Plots of the independent gradient model based on Hirshfeld partition (IGMH) for the top three lowest isomers of B₁₂H_{12-m}(OH)_m²⁻·nH₂O (m = 0, 1, 12; n = 1–6). Blue, green, and red color represents the strong electrostatic interaction, the weak van der Waals interaction, and the strong repulsive interaction, respectively. Relative energies of isomers 2 and 3 (with respect to the most stable isomer 1 in kcal/mol) calculated at DLPNO-CCSD(T)/aug-cc-pVTZ are listed for each isomer.

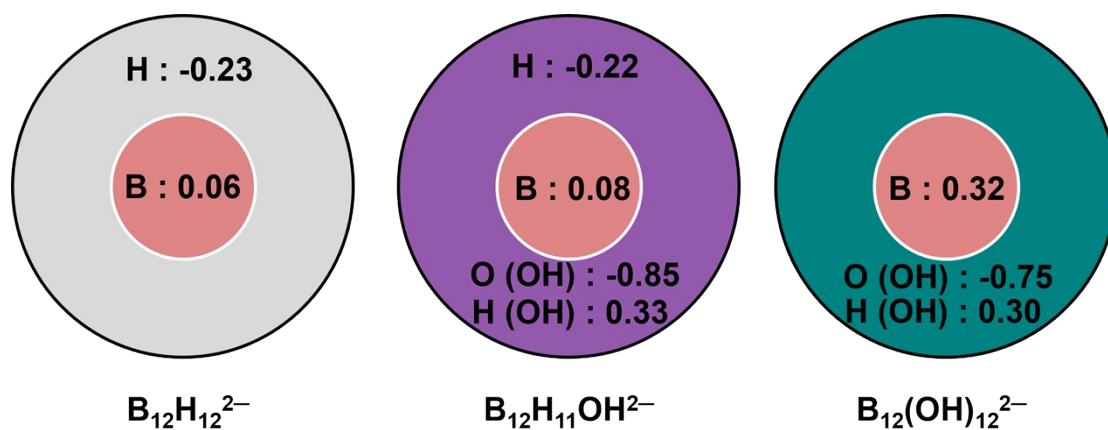
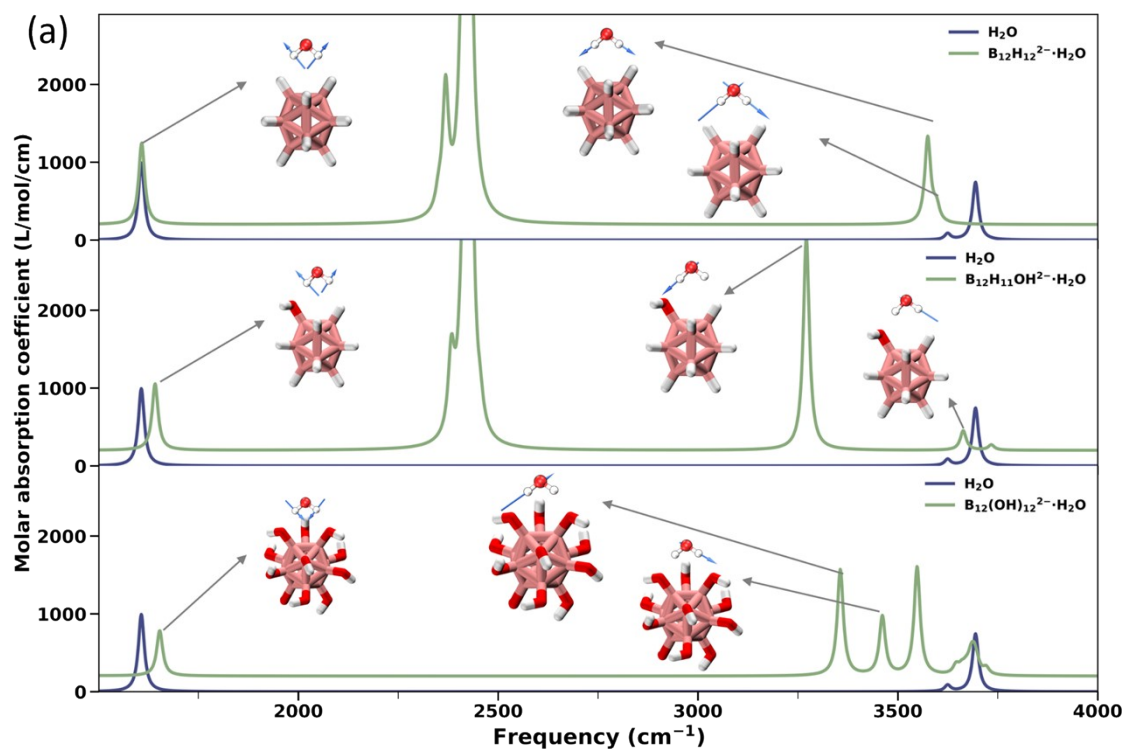


Fig. S4. Averaged restrained electrostatic potential charge (RESP charge) of atoms in $B_{12}H_{12-m}(OH)_m^{2-}$ ($m = 0, 1, 12$) cluster calculated at the PBE0/aug-cc-pVTZ level and the averaged charge of each element is also labeled.

		H ₂ O	2H ₂ O	3H ₂ O	4H ₂ O	5H ₂ O	6H ₂ O
$B_{12}H_{12}^{2-}$							
		B : 92%	B : 92%	B : 92%	B : 92%	B : 92%	B : 90%
$B_{12}H_{11}OH^{2-}$							
		B : 71%	B : 75%	B : 78%	B : 80%	B : 81%	B : 80%
$B_{12}(OH)_{12}^{2-}$							
		B : 64%	B : 64%	B : 63%	B : 63%	B : 63%	B : 62%

Fig. S5. HOMO of $B_{12}H_{12-m}(OH)_m^{2-} \cdot nH_2O$ ($m = 0, 1, 12$; $n = 0-6$) based on the lowest-lying energy anionic structures of each cluster. The contribution of boron shell to HOMOs were labeled.



(b)

Bend 1607.4 cm ⁻¹	Symmetric stretch 3624.6 cm ⁻¹	Asymmetric Stretch 3694.3 cm ⁻¹

Fig. S6. (a) Simulated vibrational spectra and specific vibrational modes of $B_{12}H_{12}(OH)_m^{2-} \cdot H_2O$ ($m = 0, 1, 12$) (in green line) along with the isolated H_2O (in blue line). (b) Three typical vibrational modes of bend, symmetries stretch and asymmetric stretch for isolated H_2O .

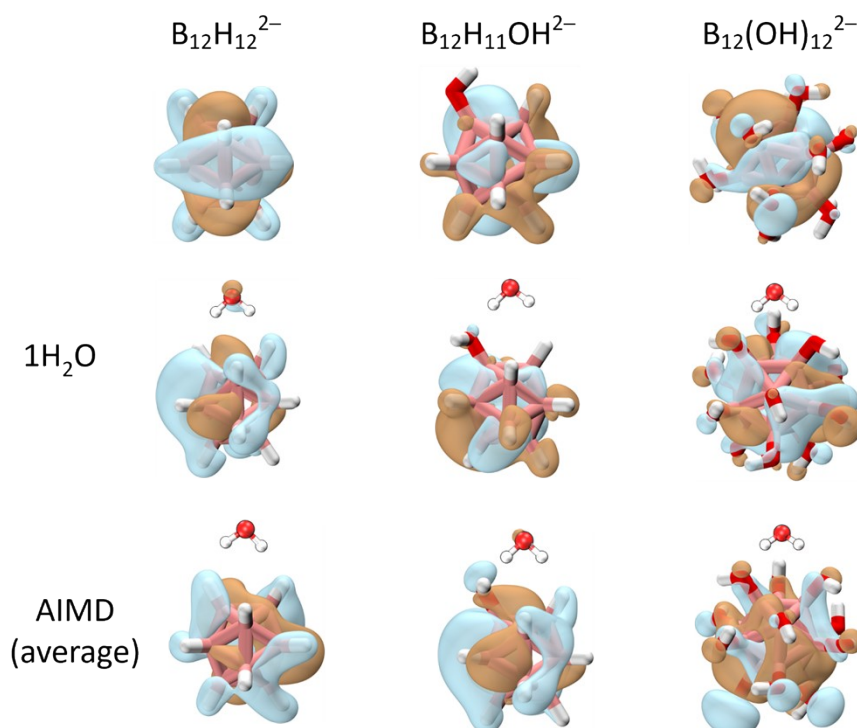


Fig. S7. The layout of excess electron (2 e) in $B_{12}H_{12-m}(OH)_m^{2-} \cdot nH_2O$ ($m = 0, 1, 12$; $n = 0, 1$) based on localized orbitals (isovalue = 0.01).

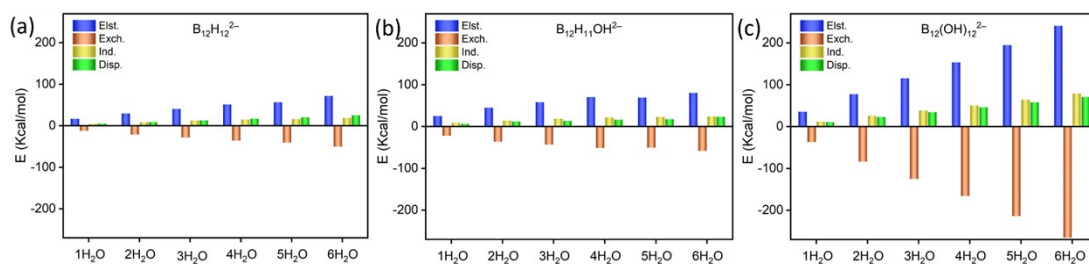


Fig. S8. (a, b, c) Electrostatic (Elst.), exchange (Exch.), induction (Ind.), and dispersion (Disp.) terms (kcal/mol) derived from energy decomposition analysis for $B_{12}H_{12-m}(OH)_m^{2-} \cdot nH_2O$ ($m = 0, 1, 12$; $n = 1-6$) at the SAPT2+/aug-cc-pVDZ level.

SI References

- 1 T. Lu, *Sobtop*, Version 1.0(dev3.1); 2023.
- 2 M. J. Abraham, T. Murtola, R. Schulz, S. Páll, J. C. Smith, B. Hess and E. Lindahl, *SoftwareX*, 2015, **1-2**, 19-25.
- 3 H. J. C. Berendsen, J. R. Grigera and T. P. Straatsma, *J. Phys. Chem.*, 1987, **91**, 6269-6271.
- 4 G. Bussi, D. Donadio and M. Parrinello, *J. Chem. Phys.*, 2007, **126**, 014101.
- 5 H. J. C. Berendsen, J. P. M. Postma, W. F. van Gunsteren, A. DiNola and J. R. Haak, *J. Chem. Phys.*, 1984, **81**, 3684-3690.
- 6 B. Hess, H. Bekker, H. J. C. Berendsen and J. G. E. M. Fraaije, *J. Comput. Chem.*, 1997, **18**, 1463-1472.
- 7 U. Essmann, L. Perera, M. L. Berkowitz, T. Darden, H. Lee and L. G. Pedersen, *J. Chem. Phys.*, 1995, **103**, 8577-8593.
- 8 F. Neese, *Wires Comput. Mol. Sci.*, 2022, **12**, e1606.
- 9 J. G. Brandenburg, C. Bannwarth, A. Hansen and S. Grimme, *J. Chem. Phys.*, 2018, **148**, 064104.